Numerical modelling of the mechanical behaviour of tetraxial technical textiles

Mehdi Ghazimoradi, Naïm Naouar, Valter Carvelli, Philippe Boisse

▶ **To cite this version:**

Mehdi Ghazimoradi, Naïm Naouar, Valter Carvelli, Philippe Boisse. Numerical modelling of the mechanical behaviour of tetraxial technical textiles. Journal of Materials Science, 2019, 54 (4), pp.3632-3647. 10.1007/s10853-018-3084-8 . hal-02174568

HAL Id: hal-02174568
https://hal.science/hal-02174568v1

Submitted on 10 Oct 2024

HAL is a multi-disciplinary open access archive for the deposit and dissemination of scientific research documents, whether they are published or not. The documents may come from teaching and research institutions in France or abroad, or from public or private research centers.

L'archive ouverte pluridisciplinaire **HAL**, est destinée au dépôt et à la diffusion de documents scientifiques de niveau recherche, publiés ou non, émanant des établissements d'enseignement et de recherche français ou étrangers, des laboratoires publics ou privés.

Numerical modelling of the mechanical behaviour of tetraxial technical textiles

Mehdi Ghazimoradi[1], Naim Naouar[2], Valter Carvelli[1,*], and Philippe Boisse[2]

[1] *Department A.B.C., Politecnico di Milano, Piazza Leonardo Da Vinci 32, 20133 Milan, Italy LaMCoS UMR 5259, INSA-Lyon,*
[2] *Université de Lyon, Villeurbanne, France*

The present study aims to numerically predict the mechanical behaviour at the meso-scale of a multiaxial textile, named tetraxial. It has warp, weft, and two diagonal yarns oriented at symmetrical angles (typically ± 45°) interlaced in the same weaving process. The flexibility of the manufacturing technique could allow for hybrid distribution of the yarn materials and, as a consequence, a wide range of mechanical behaviour. For an accurate modelling, a hyperelastic con-stitutive model of the fibrous yarns was considered to account for the peculiar nonlinear behaviour of the textile. The modelling of the tetraxial representative volume allowed predicting the mechanical response for uniaxial and biaxial tensile tests. The comparison of FE analyses with the experimental measure-ments highlights the accuracy of the numerical model to predict the nonlinear behaviour of the tetraxial textiles.

Accepted Manuscript

Introduction

Numerical simulation is a powerful tool to predict the mechanical behaviour of technical textiles, as demonstrated in the last decade by several studies [1–6]. Finite element (FE) analyses of technical fibrous materials consisting of interlacements of fibre bundles (yarns) can be performed at three scales (Fig. 1): (1) microscopic scale, the scale for the interaction of fibres in the bundle ($\approx$ 10–30 μm); (2) mesoscopic scale, the scale for the interaction of the yarns in the interlacement ($\approx$ 0.1–1 mm); and (3) macroscopic scale, the size of the sample of an application ($>$ 0.1 m).

Woven technical textiles with special architecture have received considerable attention in the literature [7–10], due to their mechanical behaviour allowing for peculiar tear resistance as well as improved formability characteristics. Two-dimensional (2D) and three-dimensional (3D) textile architectures can be considered in the classification of technical fibrous materials. For instance, triaxial braiding produces a 2D architecture with three interlaced yarns; such textiles have axial yarns in the longitudinal direction and the braided yarns tilted at an angle ranging from 30° to 60° with respect to the previous ones [11]. Advantages of triaxial braided textiles are geometry flexibility and good tear resistance. Increasing the number of weaving direction to four, a 2D multiaxial

Address correspondence to E-mail: valter.carvelli@polimi.it

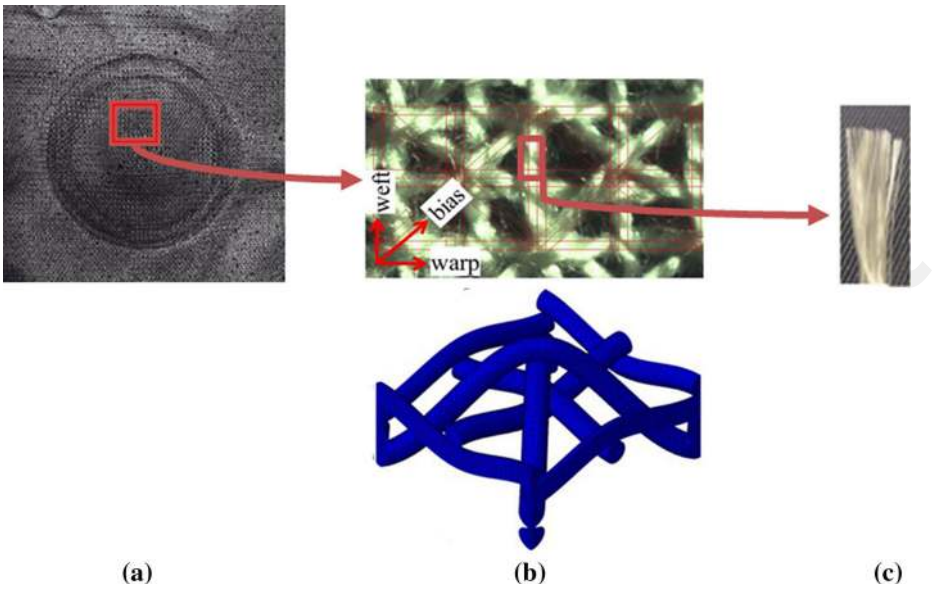

Figure 1 The three different scales for technical textiles. **a** Macroscopic scale, **b** mesoscopic scale of a tetraxial textile and its unit cell, **c** microscopic scale.

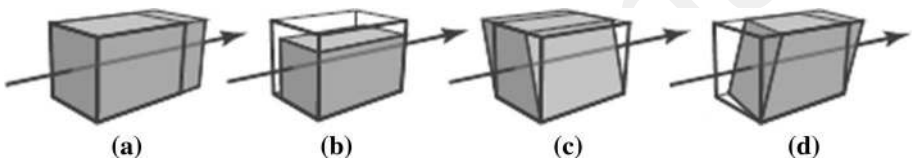

Figure 2 Four deformation modes of a yarn: **a** elongation, **b** compaction of the cross section, **c** distortion and **d** longitudinal shear.

textile is obtained, named tetraxial. The textile architecture combines a traditional orthogonal interlacement with two additional threads (bias), which can be oriented at different angles with respect to the warp/weft direction (Fig. 1b). It has warp, weft, and two diagonal yarns oriented at symmetrical angles with respect to the warp direction. In the present work, a novel loom [12] was used for manufacturing tetraxial technical textiles.

Due to the large number of possible configurations in manufacturing tetraxial hybrid technical textiles, a numerical model is an alternative to time-consuming experimental measurements to predict and assess the mechanical behaviour upon variation of several parameters, namely yarns material, spacing in the four directions and orientation of diagonals. During last decade, several meso-scale finite element (FE) models to predict the mechanical performance of technical fibrous materials have been developed based on different constitutive models [13–17]. Some mesoscopic analyses of the woven unit cell have been set up based on a hypoelastic behaviour of the yarns [18]. The hypoelastic models use an objective derivative, i.e. a derivative in a frame as close as possible of the fibre orientation, which is not easy to introduce in standard finite element codes. Developing of hyperelastic constitutive models can avoid such drawback. It was demonstrated by the hyperelastic model presented in [19–21].

The latter is adopted here for the numerical modelling of the considered tetraxial technical textiles at the meso-scale considering the representative volume (RV) of the textile. To comply with the supposed periodicity of the interlacement, periodic boundary conditions have to be enforced, as well as the contact between neighbouring yarns. The mesoscopic FE model of the tetraxial RV allowed simulating the mechanical response for in-plane uniaxial and biaxial loadings.

Within this context, the aims of this contribution are: (1) simulation of the mechanical behaviour of the yarns and hybrid tetraxial technical textiles, (2) assessment of the accuracy of the meso-scale FE model to predict the nonlinear behaviour of the textile for any in-plane loading condition by available experimental measurements, and (3) understanding

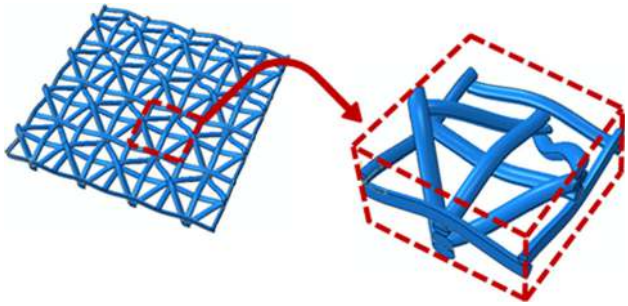

Figure 3 Representative volume (RV) of a tetraxial textile.

the peculiarities of internal stress and strain distribution.

The hyperelastic constitutive model for the yarns

The yarn is an assembly of fibres oriented in the same direction. The textile manufacturing conditions (e.g. yarns tensioning) and the interlacement considerably limit the movement of the fibres in the yarn. Hence, the yarn can be considered as a compact, homogeneous, and continuum material. The deformation of a homogeneous yarn can be considered as combination of four modes, namely elongation, compaction, distortion, and longitudinal shear (Fig. 2).

Constitutive equation for the yarn

The deformation of a homogeneous yarn can be modelled by a hyperelastic material model [22, 23]. An elastic strain energy potential per unit volume w must exist which only depends on the current strain state. Besides, assuming (1) reversible behaviour of materials, (2) no dissipate energy, and (3) fulfilment of Clausius–Duhem inequality, the constitutive equation of a hyperelastic material is written as:

$$\underline{\underline{S}}\left(\underline{\underline{F}}\right) = 2\frac{\partial w\left(\underline{\underline{F}}\right)}{\partial \underline{\underline{C}}} \tag{1}$$

where $\underline{\underline{F}}$ is the deformation gradient tensor and $\underline{\underline{S}}$ is the second Piola–Kirchhoff stress tensor. In addition, the potential energy can be written as a function of the right Cauchy–Green strain tensor $\underline{\underline{C}}$:

$$w = w\left(\underline{\underline{C}}\right) \text{ with } \underline{\underline{C}} = \underline{\underline{F}}^T \cdot \underline{\underline{F}} \tag{2}$$

The tensor $\underline{\underline{C}}$ has three invariants:

$$I_1 = Tr(\underline{\underline{C}}),\ I_2 = \frac{1}{2}\left(Tr(\underline{\underline{C}})^2 - Tr(\underline{\underline{C}}^2)\right),\ I_3 = \det \underline{\underline{C}} \tag{3}$$

The Jacobin $J = \sqrt{I_3} = \det \underline{\underline{F}}$ describes the local volume change during the deformation.

The parallel fibres in a yarn can be considered as a transversally isotropic material. A unit vector $\underline{M}$ in the direction of the fibre makes possible the definition of a structural tensor [24]:

$$\underline{\underline{M}} = \underline{M} \otimes \underline{M} \tag{4}$$

For transversal isotropic materials [25, 26], the strain energy density function is a function of the three invariants of $\underline{\underline{C}}$ and of two mixed invariants defined from the structural tensor $\underline{\underline{M}}$:

$$w = w(I_1, I_2, I_3, I_4, I_5) \tag{5}$$

$$I_4 = \underline{\underline{C}} : \underline{\underline{M}} \quad I_5 = \underline{\underline{C}}^2 : \underline{\underline{M}} \tag{6}$$

Strain energy function of the different deformation modes

Physically based invariants, i.e. invariants directly related to the deformation modes of the yarns (Fig. 2), are considered [19]. I_{elong} is the elongation invariant in the direction of the fibres. I_{comp} is the transverse compaction, I_{dist} is the distortion (change of angle) in the transverse section, and I_{sh} is the shear along the fibre direction.

Table 1 Geometric features of the tetraxial textiles PET/PET/PET and PET/Aramid/PET RV in mm (average and standard deviation of 5 measurements)

	Length	Width	Thickness
Tetraxial	4 ± 0.05	3.66 ± 0.04	1.6 ± 0.05

Table 2 Some properties of the yarns

Material	Count (tex)	Nominal strength (cN/tex)
Polyester (PET)	63	20
Aramid	130	219

Accepted Manuscript

Table 3 Characteristics of the tetraxial textiles

Yarns (warp/weft/bias)	Areal density (g/m^2)	Warp (ends/cm)	Weft (picks/cm)	Bias (threads/cm)
PET/PET/PET	136	6	7	5
PET/Aramid/PET	159	6	7	5

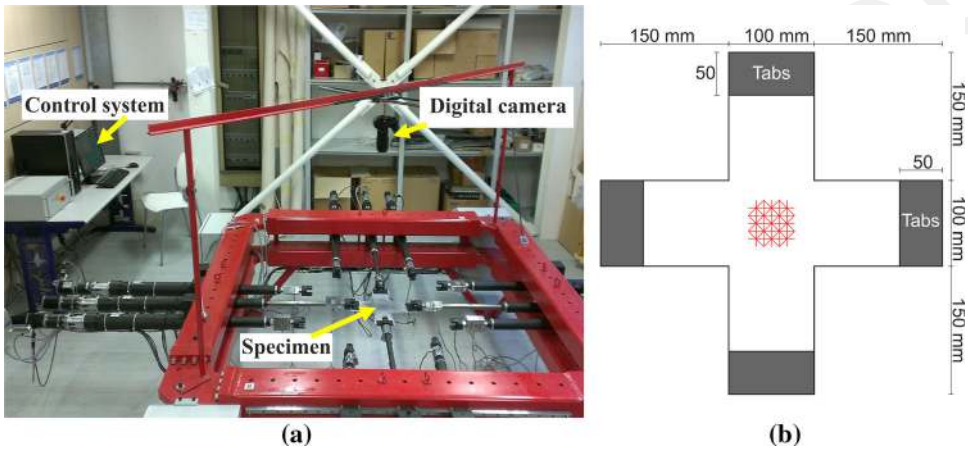

Figure 4 **a** Device for biaxial tensile tests, **b** cross-shaped specimen.

These physically based invariants are function of the invariants defined in Eqs. (3) and (6):

$$I_{\text{elong}} = \frac{1}{2}\ln(I_4), \quad I_{\text{comp}} = \frac{1}{4}\ln\left(\frac{I_3}{I_4}\right),$$
$$I_{\text{dist}} = \frac{1}{2}\ln\left(\frac{I_1 I_4 - I_5}{2\sqrt{I_3 I_4}} + \sqrt{\left(\frac{I_1 I_4 - I_5}{2\sqrt{I_3 I_4}}\right)^2 - 1}\right), \quad I_{\text{sh}} = \sqrt{\frac{I_5}{I_4^2} - 1} \tag{7}$$

They are used to define the strain energy potential

$$w\left(\underline{\underline{C}}\right) = w\left(I_{\text{elong}}, I_{\text{comp}}, I_{\text{dist}}, I_{\text{sh}}\right) \tag{8}$$

Elongation strain energy

The strain energy functions corresponding to the linear ($I_{\text{elong}} > I^0_{\text{elong}}$) and nonlinear ($I_{\text{elong}} \le I^0_{\text{elong}}$) parts of the elongation behaviour of the yarn are, respectively, defined by:

$$w^{\text{lin}}_{\text{elong}} = \frac{K_{\text{elong}} - K^0_{\text{elong}}}{6S_0}\left(I^0_{\text{elong}}\right)^2 - \frac{K_{\text{elong}} - K^0_{\text{elong}}}{2S_0}\left(I^0_{\text{elong}} I_{\text{elong}}\right) + \frac{K_{\text{elong}}}{2S_0}\left(I^2_{\text{elong}}\right) \tag{9}$$

$$w^{\text{nl}}_{\text{elong}} = \frac{K^0_{\text{elong}}}{2S_0}\left(I^2_{\text{elong}}\right) + \frac{K_{\text{elong}} - K^0_{\text{elong}}}{6S_0 I^0_{\text{elong}}}\left(I^3_{\text{elong}}\right) \tag{10}$$

The second tensile Piola–Kirchhoff tensor $\underline{\underline{S}}_{\text{elong}}$ is:

$$\underline{\underline{S}}_{\text{elong}} = \frac{1}{4}\underline{\underline{M}}\begin{cases} \frac{K^0_{\text{elong}}}{S_0}\left(I_{\text{elong}}\right) + \frac{K_{\text{elong}} - K^0_{\text{elong}}}{2S_0 I^0_{elong}}\left(I^2_{\text{elong}}\right) & \text{if} \quad I_{\text{elong}} \le I^0_{\text{elong}} \\ -\frac{K_{\text{elong}} - K^0_{\text{elong}}}{2S_0}\left(I^0_{\text{elong}}\right) + \frac{K_{\text{elong}}}{S_0}\left(I_{\text{elong}}\right) & \text{if} \quad I_{\text{elong}} > I^0_{\text{elong}} \end{cases} \tag{11}$$

The strain potential energy is defined by three parameters: I^0_{elong},K^0_{elong},K_{elong}. They are identified by a tensile test on a single yarn.

Compaction strain energy

A power-based strain energy function was proposed [19]:

$$w_{\text{comp}} = \begin{cases} K_{\text{comp}}\left|I_{\text{comp}}\right|^p & \text{if} \quad I_{\text{comp}} \le 0 \\ 0 & \text{if} \quad I_{\text{comp}} > 0 \end{cases} \tag{12}$$

It is assumed that no energy is required for yarn section expansion. Accordingly, the second Piola–Kirchhoff stress tensor is:

$$\underline{\underline{S}}_{\text{comp}}\left(I_{\text{comp}} \le 0\right) = -\frac{P}{2}K_{\text{comp}}\left|I_{\text{comp}}\right|^{p-1}\left(\underline{\underline{C}}^{-1} - \frac{1}{I_4}\underline{\underline{M}}\right) \tag{13}$$

The parameters to be identified are then $K_{\text{comp}}$and p. An inverse method was here adopted in the case of an equi-biaxial tensile test on a woven fabric to

Accepted Manuscript

Figure 5 Identification of the model elongation parameters for: **a** PET yarn, **b** Aramid yarn.

Identification parameters for yarn elongation	
$S_0\ (mm^2)$	0.146
I^0_{elong}	0.003724
$K^0_{elong}\ (N)$	2477
$K_{elong}\ (N)$	867

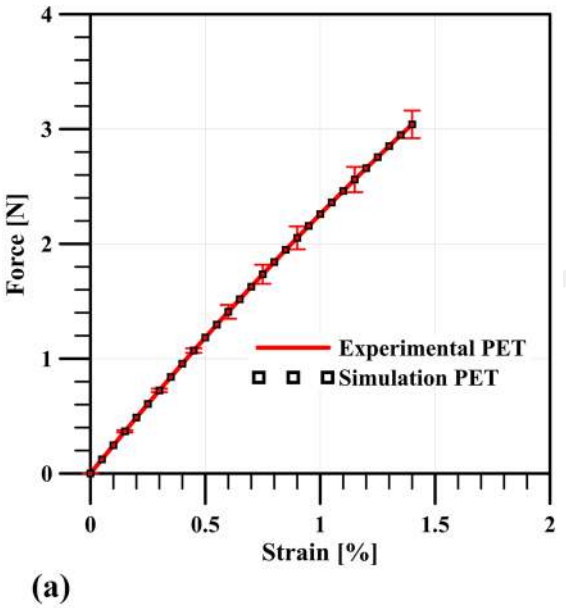

(a)

Identification parameters for yarn elongation	
$S_0\ (mm^2)$	0.146
I^0_{elong}	0.1353
$K^0_{elong}\ (N)$	81748
$K_{elong}\ (N)$	1835074

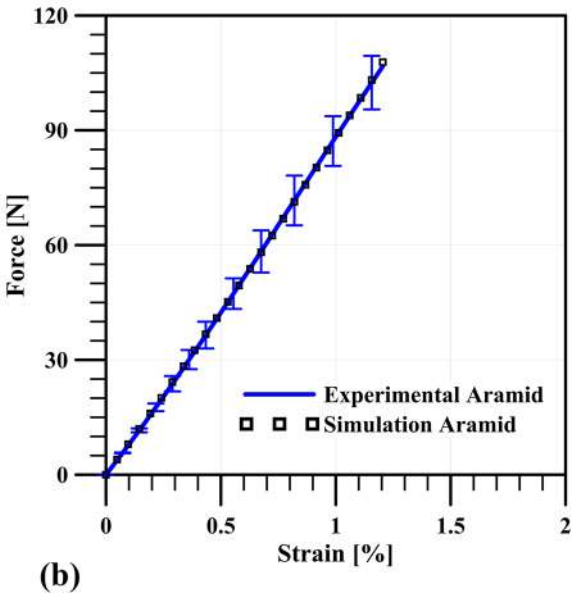

(b)

identify K_{comp} and p, and also the parameter K_{dist} (see below).

Distortion strain energy

In the numerical investigation, the distortion stiffness is assumed constant which leads to the following strain energy function:

$$w_{\text{dist}} = \frac{1}{2} K_{\text{dist}} I_{\text{dist}}^2 \tag{14}$$

The second Piola–Kirchhoff stress tensor associated with this distortion strain energy is then:

$$\underline{\underline{S}}_{\text{dist}} = 2K_{\text{dist}} I_{\text{dist}} \times \frac{2I_4 \underline{\underline{I}} - (I_1 I_4 - I_5)\underline{\underline{C}}^{-1} + \left(I_1 + \frac{I_5}{I_4}\right)\underline{\underline{M}} - 2\left(\underline{\underline{C}} \cdot \underline{\underline{M}} + \underline{\underline{M}} \cdot \underline{\underline{C}}\right)}{4\sqrt{(I_1 I_4 - I_5)^2 - 4I_3 I_4}} \tag{15}$$

The parameter K_{dist} is identified by the inverse method in the case of an equi-biaxial tensile test, at the same time as the compaction parameters.

Longitudinal shear strain energy

A linear elastic behaviour is assumed for this deformation mode, which induces the following strain energy potential:

Identification parameters for compaction	
$K_{comp}\ (N)$	14500
p_{comp}	3.2

Identification parameter for distortion	
$K_{dist}\ (MPa)$	0.035

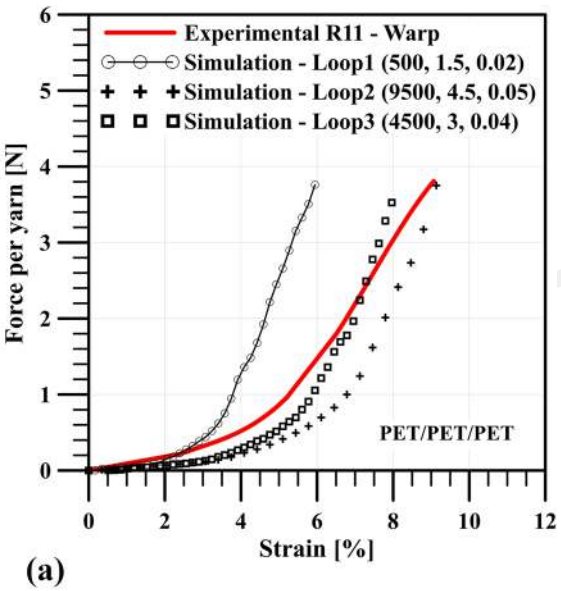

Identification parameters for compaction	
$K_{comp}\ (N)$	16500
p_{comp}	7

Identification parameter for distortion	
$K_{dist}\ (MPa)$	0.066

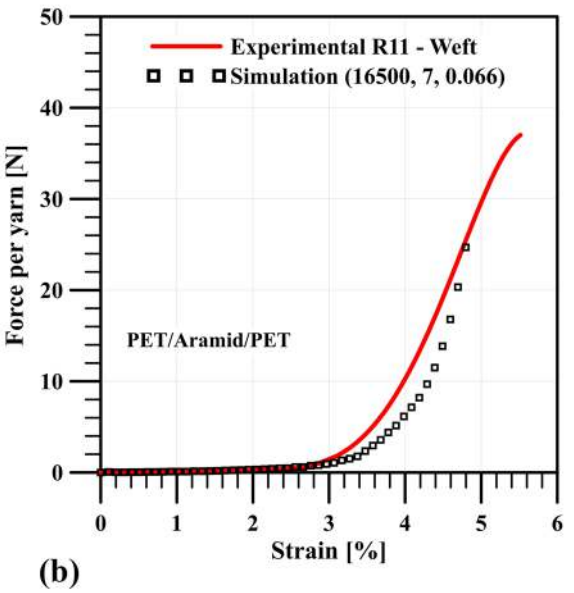

Figure 6 Identification of the model compaction and distortion parameters by equi-biaxial tension test of: **a** PET/PET/PET, **b** PET/Aramid/PET tetraxial textile.

$$w_{\mathrm{sh}} = \frac{1}{2} K_{\mathrm{sh}} I_{\mathrm{sh}}^2 \tag{16}$$

The second Piola–Kirchhoff stress tensor is then:

$$\underline{\underline{S}}_{\mathrm{sh}} = \frac{1}{2} K_{\mathrm{sh}} \left[\frac{1}{I_4^2} \left(\underline{\underline{C}} \cdot \underline{\underline{M}} + \underline{\underline{M}} \cdot \underline{\underline{C}} \right) - \frac{2 I_5}{I_4^3} \underline{\underline{M}} \right] \tag{17}$$

The parameter K_{sh} is identified by an uniaxial tensile test of the fabric whose elongation parameters have been previously determined.

Combination of all deformation modes

Each contribution of deformation mode is considered as independent from the others. Therefore,

$$\begin{aligned} \underline{\underline{S}} &= 2 \left(\frac{\partial w_{\mathrm{elong}}}{\partial I_{\mathrm{elong}}} \frac{\partial I_{\mathrm{elong}}}{\partial \underline{\underline{C}}} + \frac{\partial w_{\mathrm{comp}}}{\partial I_{\mathrm{comp}}} \frac{\partial I_{\mathrm{comp}}}{\partial \underline{\underline{C}}} + \frac{\partial w_{\mathrm{dist}}}{\partial I_{\mathrm{dist}}} \frac{\partial I_{\mathrm{dist}}}{\partial \underline{\underline{C}}} + \frac{\partial w_{\mathrm{sh}}}{\partial I_{\mathrm{sh}}} \frac{\partial I_{\mathrm{sh}}}{\partial \underline{\underline{C}}} \right) \\ &= \underline{\underline{S}}_{\mathrm{elong}} + \underline{\underline{S}}_{\mathrm{comp}} + \underline{\underline{S}}_{\mathrm{dist}} + \underline{\underline{S}}_{\mathrm{sh}} \end{aligned} \tag{18}$$

The hyperplastic constitutive equation was implemented in a user material subroutine VUMAT for the finite element code ABAQUS/Explicit.

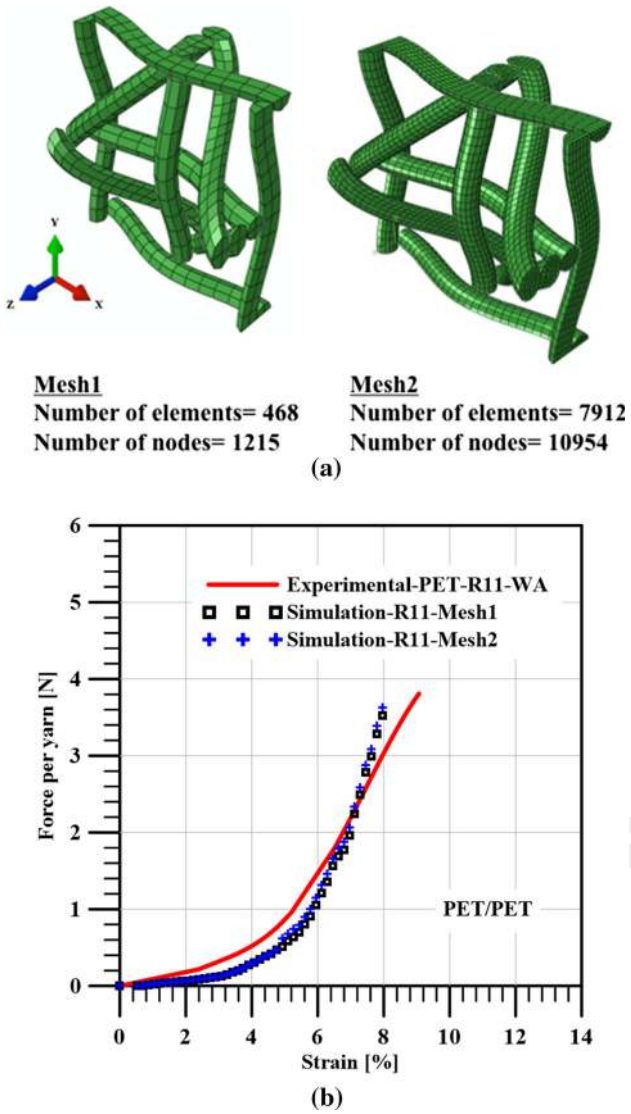

Figure 7 **a** Two meshes for PET/PET/PET tetraxial RV, and **b** effect of the mesh density on R11 biaxial tensile response, force vs strain in warp direction.

Some features of the finite element model of the tetraxial textiles

The periodic structure of the considered textiles allowed to reduce the investigation to the representative volume (RV) at meso-scale level (Fig. 3).

To reproduce the 3D geometry of the tetraxial textile, a set of geometric features were measured by optical microscope observations. In particular, yarn cross section, yarn height, length, width, and thickness of the RV are listed in Table 1. The assumptions set to create the 3D solid model of the RV were circular cross section of the yarns with the proper diameter to have the real measured section surface and constant cross section along the yarn path. The yarn was considered as a 3D continuous domain and was meshed using eight-node hexahedral elements [18, 27]. Two mesh sizes were considered and compared to assess the accuracy of predictions in section "Mesh sensitivity".

To insure periodicity, periodic boundary conditions were enforced based on [28]. Besides, the contact of the yarns in the dry textile was simulated by the contact model implemented in ABAQUS/Explicit [29]. The model considers a surface-based hard contact between the connected surfaces in normal direction and a frictional contact in the tangential ones, assuming the friction coefficient as measured in [30].

Materials and experimental characterization

Materials

Two of the tetraxial textiles studied in [30] were considered: PET/PET/PET and PET/Aramid/PET hybrid tetraxial textile (see, for example, Figure 1b). Table 2 details the feature of the yarns (PET and Aramid). Additionally, the construction of the two tetraxial technical textiles is summarized in Table 3. In the present investigation, yarn material was varied only in weft direction.

Experimental characterization

The tensile behaviour was measured with yarns extracted in warp, weft, and diagonal directions of both textiles, by an Instron device with 500 N load cell. The gauge length was 150 mm and testing speed 5 mm/min. Five tests were performed for each yarn direction.

The biaxial and uniaxial tensile mechanical behaviours of the tetraxial textiles were obtained by a home design biaxial device (see Fig. 4a, and [30]). The displacement is generated in each direction of cross-shaped specimen (Fig. 4b), which is set in the centre of the machine. Arms of the specimens had width of 100 mm to create a biaxial loaded portion of 100×100 mm^2 with an almost uniform distribution of strain on centre. All tests were performed at room temperature assuming different ratios R of the warp

Accepted Manuscript

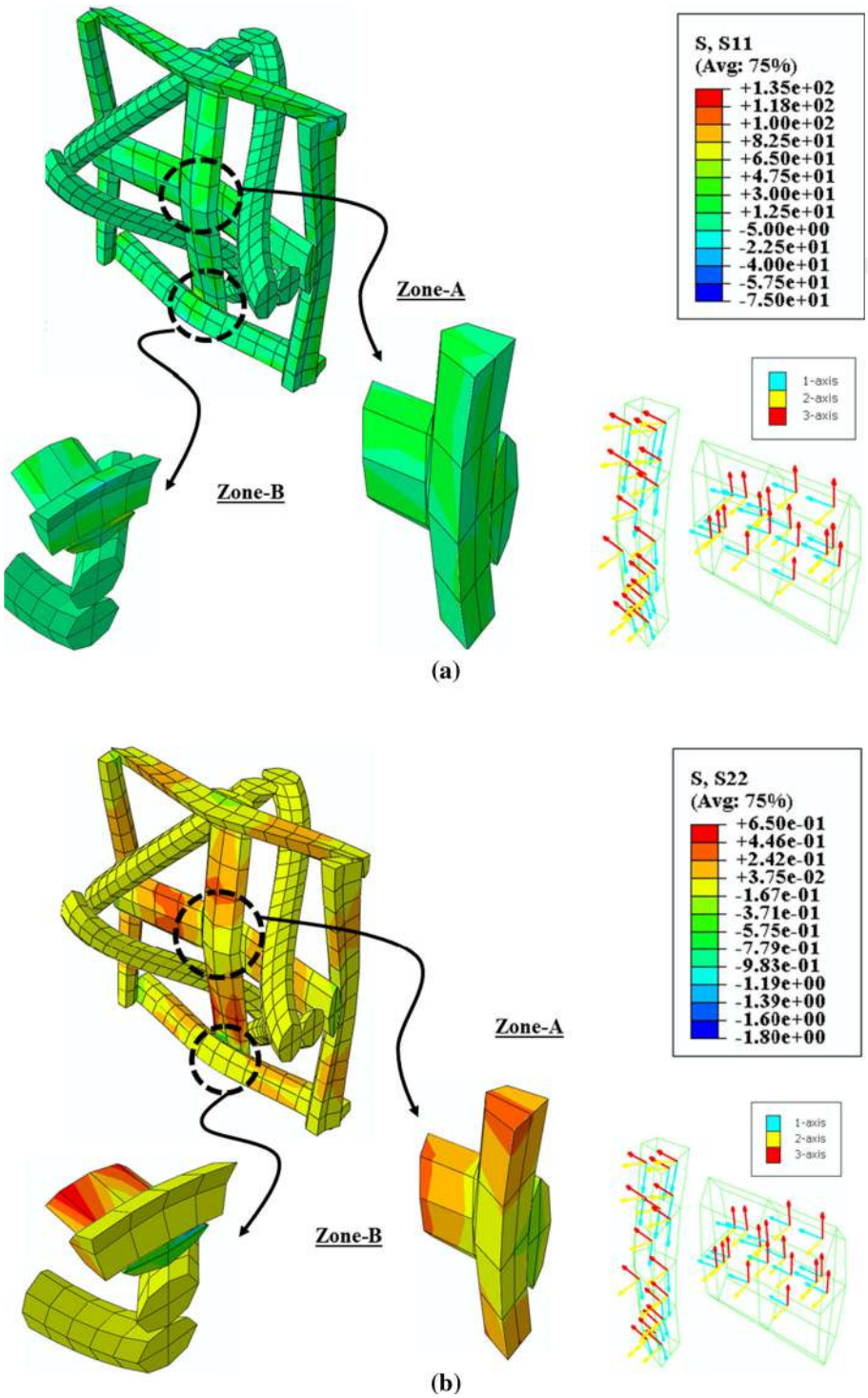

Figure 8 Map of the stress distribution for equi-biaxial loading (R11) at 1.6 N per yarn of the PET/PET tetraxial textile. Components in the local coordinate system (1, 2, 3): **a** S_{11} and **b** S_{22}.

to the weft displacement rate (e.g. R21 means a displacement rate in warp direction double than the weft one). Besides, during test, a digital camera recorded images at a frequency of 1 Hz for image correlation analysis. The full field displacement and strain were obtained by digital image correlation (DIC) technique (VIC 2D [31]).

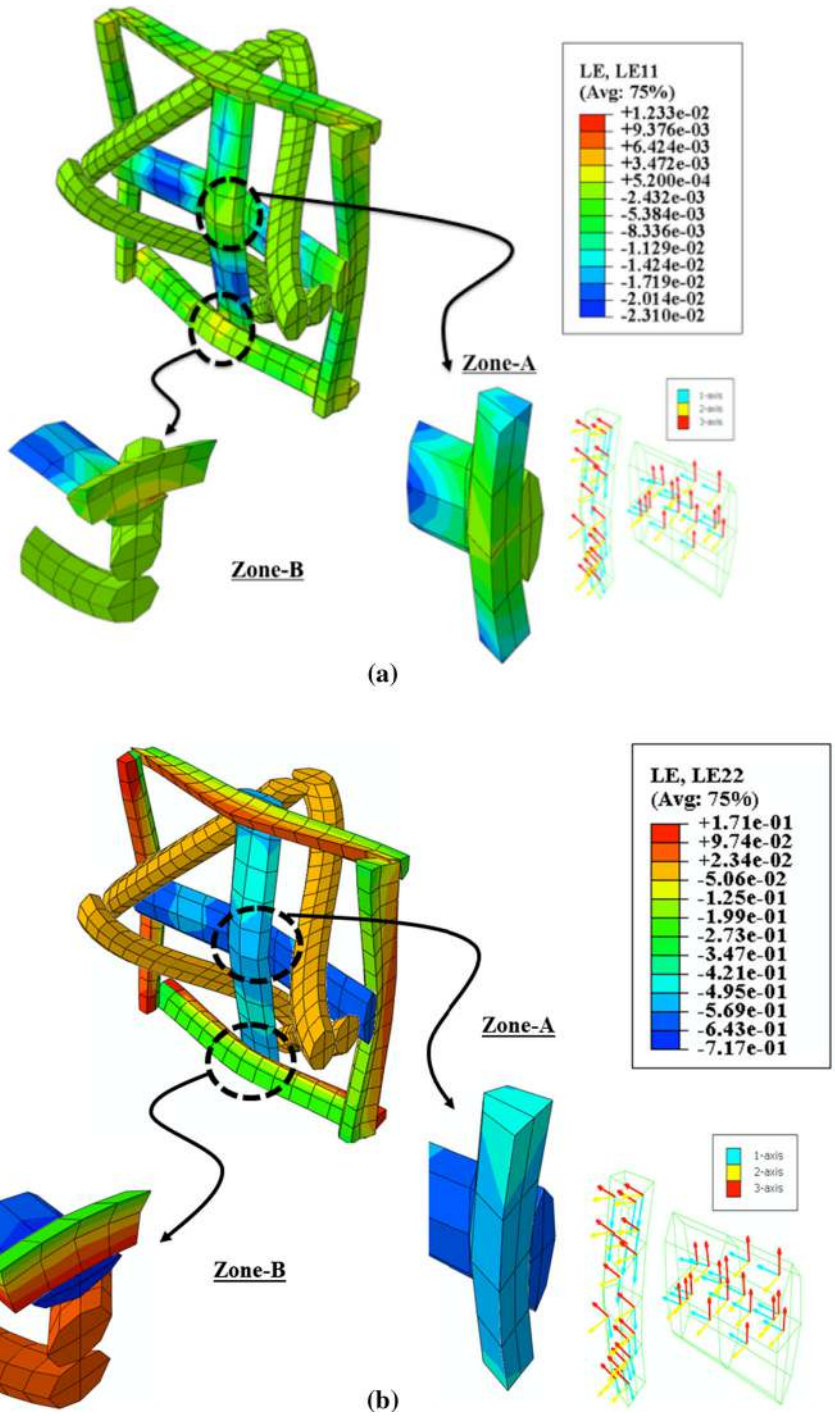

Figure 9 Map of logarithmic strain for equi-biaxial loading (R11) at 1.6 N per yarn of the PET/PET/PET tetraxial textile. Components in the local coordinate system (1, 2, 3): **a** LE_{11}, **b** transverse LE_{22}.

Results and comparisons

For each deformation mode (see Fig. 2), a strain energy density function based on the experimental behaviour of the tetraxial textile (i.e. experimental results presented in [30]) was defined. Afterwards, the strain energy density was used to identify the model parameters.

Identification of parameters for different deformations of yarn

Tensile test of yarn must be performed on a woven yarn extracted from the textile after the weaving process, to have realistic mechanical behaviour. The initial section of the yarn, S_0, was measured by optical microscope, while $I^0_{\text{elong}}, K^0_{\text{elong}}, K_{\text{elong}}$ were

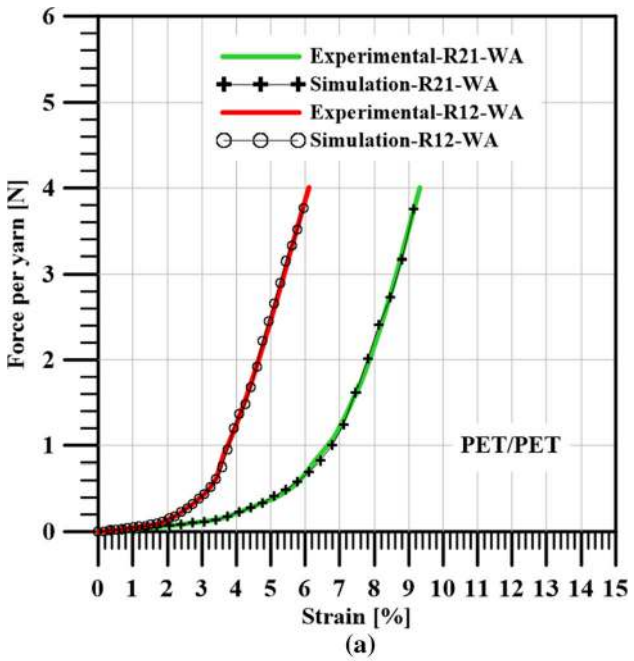

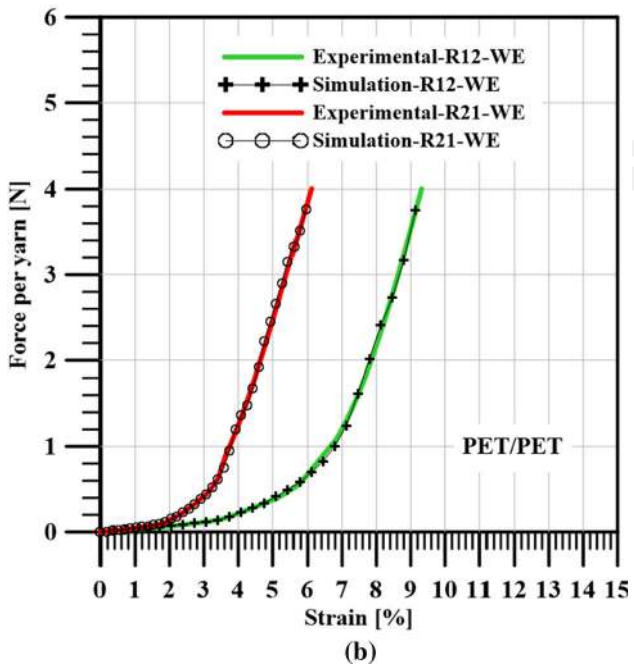

Figure 10 Comparison of experimental and numerical results for biaxial loading R12 and R21 of PET/PET/PET tetraxial technical textile. Force versus strain in: **a** warp direction and **b** weft direction.

identified by means the sum of differences squared algorithm (see Fig. 5).

The parametersK_{dist}, $K_{comp}$and p were identified by an inverse analysis based on equi-biaxial tension test (R11) of the tetraxial textiles. In an equi-biaxial tensile test, the yarn is compacted in the transverse direction due to the biaxial tension and to the weaving. This leads to changes of I_{comp} and I_{dist} and consequently to identify the parameters of the corresponding strain potentials. The inverse analysis allowed to have the equi-biaxial response very close to the measured one, with few iterations (Fig. 6). Nevertheless, the existence of local minima of the error estimation induces that the initial parameters must be close to the final solution to have convergence. This imposes an initial trial and error approach before starting the identification procedure.

The main deformation modes of fabric under tensile loading are the yarn elongation and longitudinal shear. Hence, the parameter of Eqs. (16) and (17) is identified once the parameters of the elongation behaviour of the yarn have been determined. This is justified being the strain energies associated to the elongation and longitudinal shear much greater than the compaction and distortion ones [19]. The procedure allowed to estimate the parameter K_{sh} as 3 MPa.

Meso-scale FE modelling of PET/PET tetraxial technical textile

Mesh sensitivity

Two meshes (468 and 7912 hexahedral elements, Fig. 7a) were adopted to check the mesh sensitivity considering the force versus logarithmic strain in warp direction for biaxial tensile loading. The comparison shows that one order increase in the number of elements did not have any substantial effect on the numerical prediction (Fig. 7b). The coarse mesh was considered for the other loadings simulation.

Biaxial and uniaxial loading

The first assessment of the numerical model was comparing the results of uni- and biaxial tensile loadings.

As in section "Mesh sensitivity", equi-biaxial loading of PET/PET/PET textile was used to assess the mesh sensitivity of the hyperelastic constitutive model, and numerical result had a good agreement with experimental measurements (Fig. 7b).

Figure 8 illustrates the comparison of the longitudinal and transverse stress components, in the local reference frame of the yarns, distribution in PET/PET/PET tetraxial textile during equi-biaxial loading. Two zones A and B have been detailed. Due to the

Manuscript

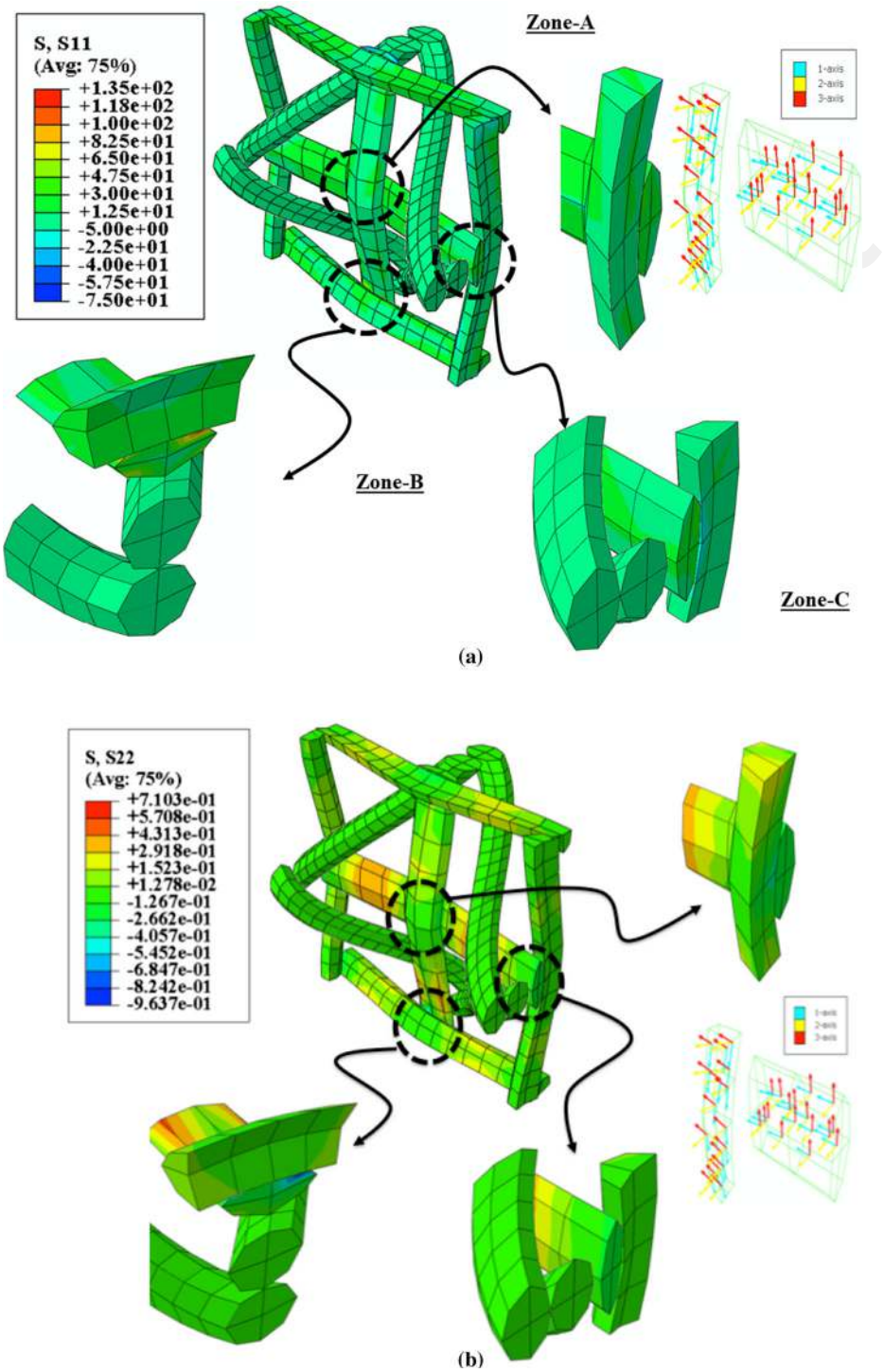

Figure 11 Map of stress distribution for biaxial loading R21 at 1.6 N per yarn of the PET/PET/PET tetraxial textile. Components in the local coordinate system (1, 2, 3): **a** S_{11} and **b** S_{22}.

interlacement of the tetraxial technical textile, the maximum stress concentration was estimated in the zone B (see distribution of S_{11} and S_{22} in Fig. 8). Different types of contact in tetraxial textile create different stress concentrations at meso-scale level, mainly of the longitudinal component S_{11} (axis 1), while the transverse to the textile plane component S_{22} (axis 2) did not highlight considerable variations.

On the other hand, the longitudinal and transverse logarithmic strain components, in the local reference frame of the yarns, show accordingly the maximum deformation in zone B (Fig. 9).

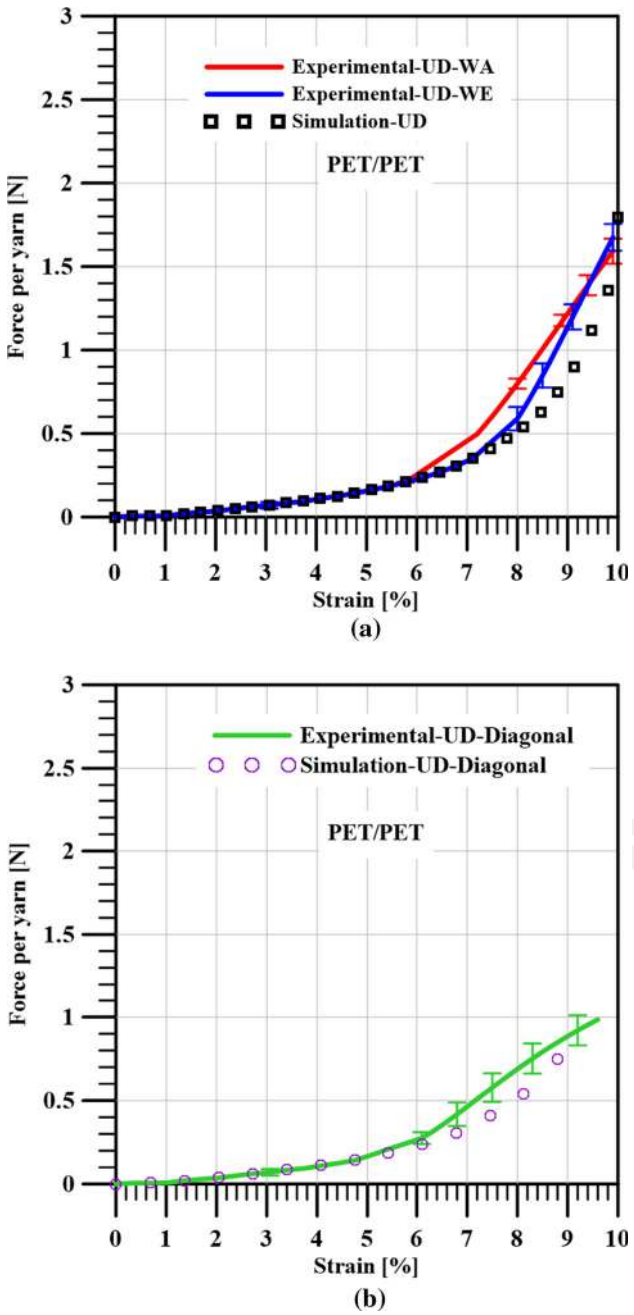

Figure 12 Comparison of experimental and numerical results for uniaxial loading of PET/PET/PET tetraxial textile: (**a**) warp and weft directions, (**b**) diagonal direction.

Figure 10 presents good agreement of the numerical and experimental results for the two considered biaxial loading R12 and R21.

The distribution of stress components for the biaxial loading R21, 1.6 N per yarn, at three different locations highlights the main concentration in zone B (Fig. 11), as for equi-biaxial loading.

Uniaxial behaviour of PET/PET/PET tetraxial technical textile was simulated in warp, weft, and diagonal directions, see Fig. 12. The good agreement of experimental and numerical results is for both the first and the second branch of the curves, which have increasing stiffness. The numerical model predicts accurately the uniaxial tensile mechanical behaviour of the fabric, for both loading directions, up to a large strain level ($\sim$ 10%).

Figure 13 presents the logarithmic strain components, in the local reference frame of the yarns, for 1.8 N per yarn during uniaxial loading in warp and diagonal direction of PET/PET/PET tetraxial textile. The diagonal yarns have a significant effect on bias extension, while loading in warp direction; as expected, the diagonal yarns do not provide a contribution to the deformation of the tetraxial textile.

Meso-scale FE modelling of PET/Aramid/PET hybrid tetraxial textile

The comparison of the numerical and experimental results of biaxial loading R11 (Fig. 14) and R12 and R21 (Fig. 15) for PET/Aramid/PET hybrid tetraxial textile shows the accuracy of the model, as well as the completely different tensile behaviours in warp and weft directions.

The anisotropic behaviour of the PET/Aramid/PET hybrid textile was accurately predicted for uniaxial loading in the three yarns direction (warp, weft, and diagonal), see Fig. 16. The accuracy of the model allowed to predict the complete mechanical response for weft and warp loading up to considerable strain levels of the textile.

Conclusions

A hyperelastic constitutive model specific for fibrous yarns was adopted to simulate the mechanical behaviour of a novel tetraxial technical textile. The numerical FE analyses allowed the prediction of different combinations of materials of the yarns (PET and Aramid) and different in-plane loading conditions (uniaxial and biaxial tensile loading). The meso-scale simulations (representative volume scale) were validated by the experimental measurements, and the model showed accurate predictions of the mechanical behaviour for any loading conditions and any considered tetraxial textile.

Author Manuscript

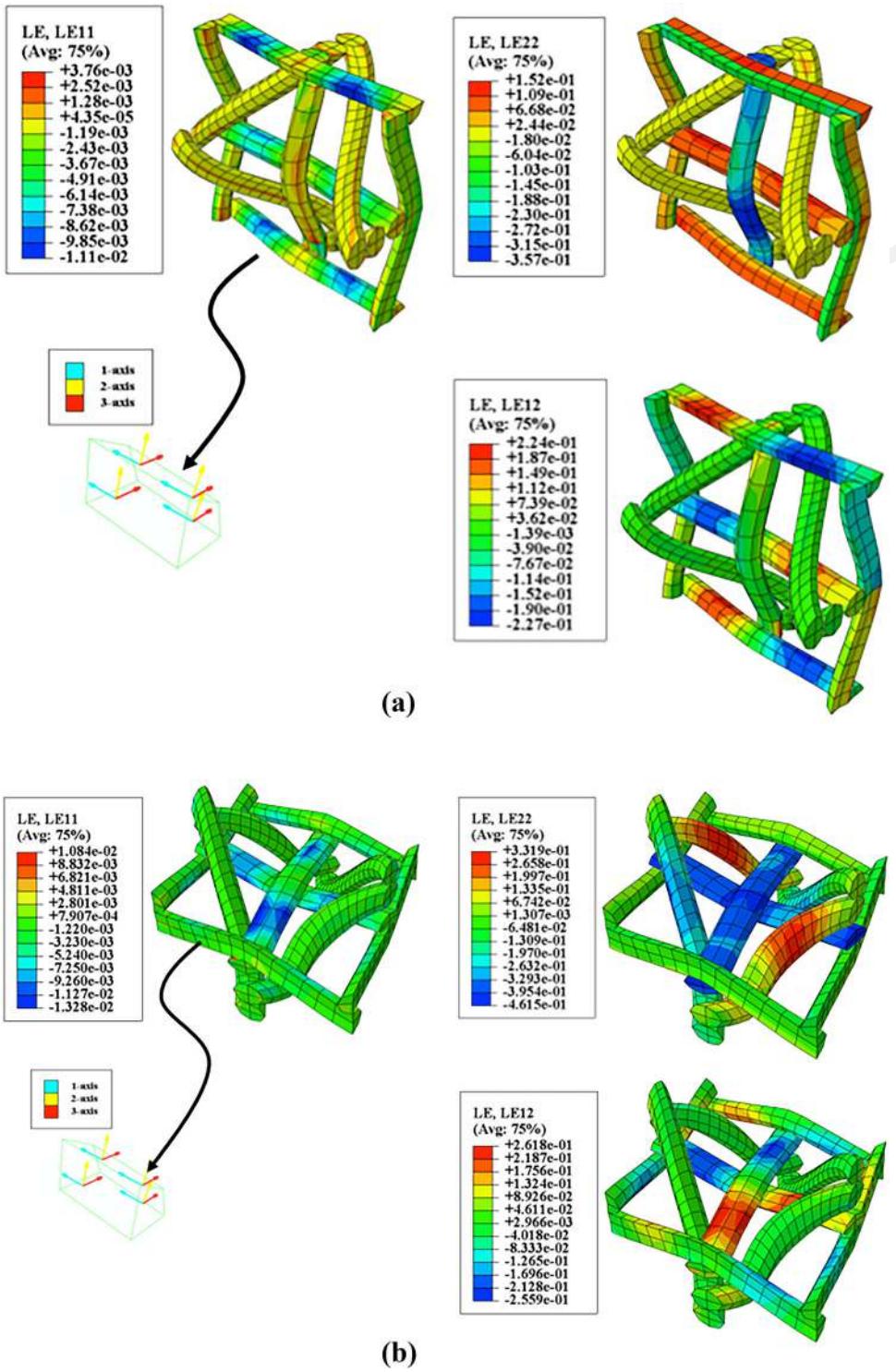

Figure 13 Map of logarithmic strain components (LE_{11}, LE_{22}. LE_{12}) in the local coordinate system (1, 2, 3) for uniaxial loading at 1.8 N per yarn, loading in: **a** warp, **b** diagonal direction.

The accuracy of the model in predicting the macro response as well as the distribution of stress and strain inside the yarns at meso-scale provides a powerful numerical tool to investigate the mechanical behaviour and to design such tetraxial textile considering the variation of the wide range of parameters (yarn material, spacing in the three yarns direction, orientation of the diagonal to the warp and weft yarns, etc.). In the design phase for any particular application, the numerical model could allow to

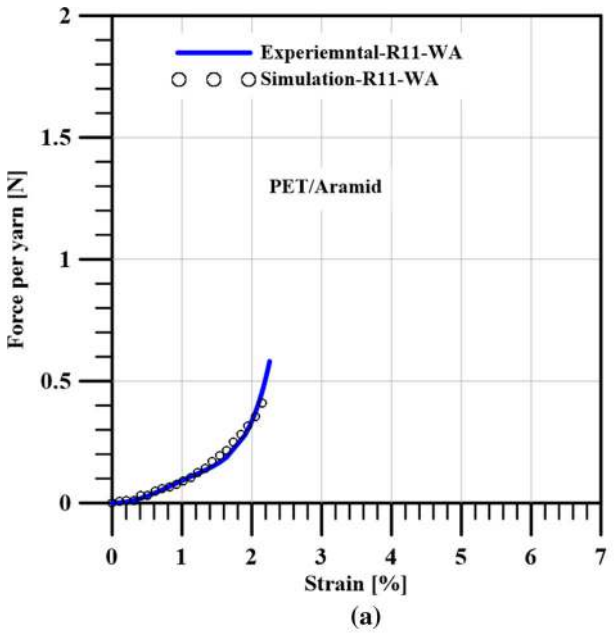

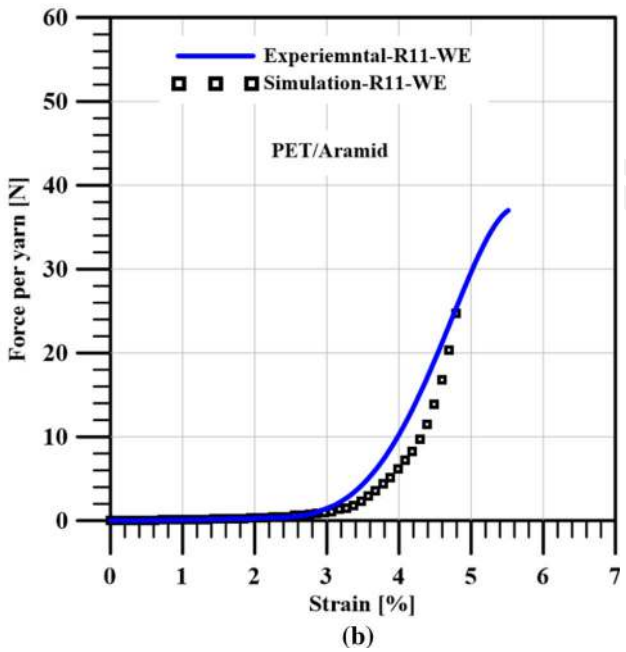

Figure 14 Comparison of experimental and numerical results for equi-biaxial loading R11 of PET/Aramid/PET hybrid textile. Force vs strain in: **a** warp, **b** weft direction.

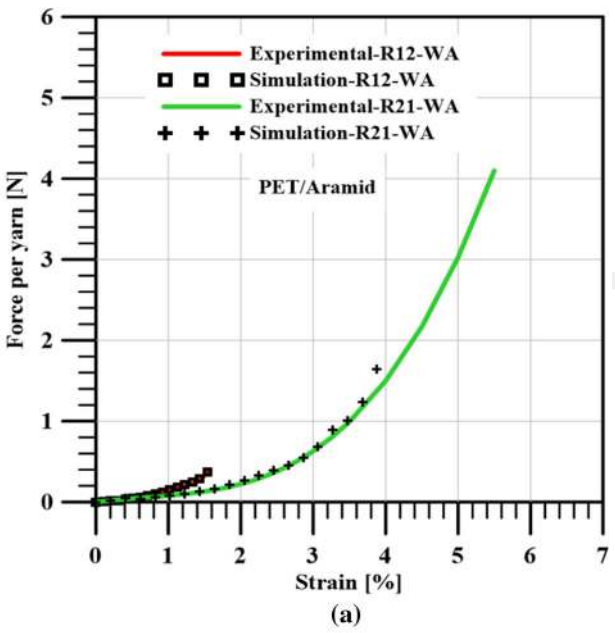

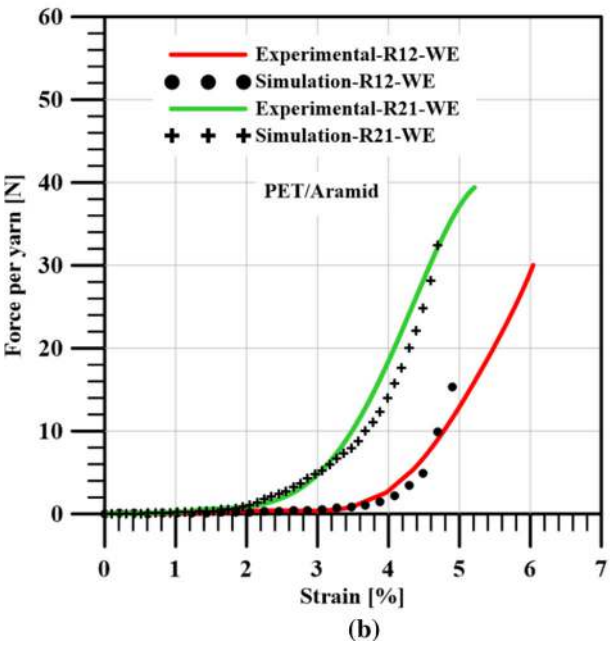

Figure 15 Comparison of experimental and numerical results for biaxial loading R12 and R21 of PET/Aramid hybrid technical textile. Force vs strain in: **a** warp, **b** weft direction.

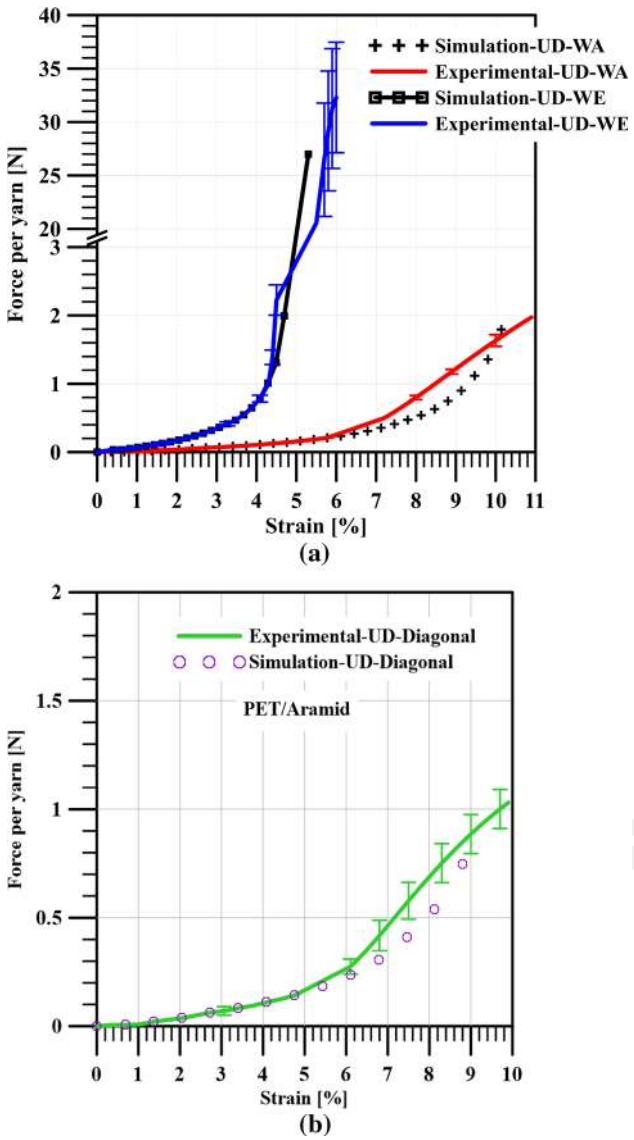

Figure 16 Comparison of experimental and numerical results for uniaxial loading of PET/Aramid/PET tetraxial textile. Force vs strain in: **a** warp and weft directions, **b** diagonal direction.

reduce the time for manufacturing trials, and time and cost for experimental characterizations.

The future developments of the tetraxial loom will provide tetraxial textiles suitable as reinforcement of composite materials. Hence, the present numerical model will be adopted to predict the performance of the tetraxial reinforcements before the weaving manufacturing and will be extended to predict the mechanical properties of the tetraxial textile reinforced polymer composites.

Acknowledgements

The work was supported by the Italian Ministry of Economic Development under the research project 'Tetraxial' (Grant No. MI01_00202).

References

[1] Peng X, Cao J (2002) A dual homogenization and finite element approach for material characterization of textile composites. Compos B 33(1):45–56

[2] Boisse P, Gasser A, Hagege B, Billoet JL (2005) Analysis of the mechanical behavior of woven fibrous material using virtual tests at the unit cell level. J Mater Sci 40:5955–5962. https://doi.org/10.1007/s10853-005-5069-7

[3] Green SD, Matveev MY, Long AC, Ivanov D, Hallett SR (2014) Mechanical modelling of 3D woven composites considering realistic unit cell geometry. Compos Struct 118:284–293

[4] Moustaghfir N, Jeguirim SEG, Durville D, Fontaine S, Wagner-Kocher C (2013) Transverse compression behavior of textile rovings: finite element simulation and experimental study. J Mater Sci 48:462–472. https://doi.org/10.1007/s10853-012-6760-0

[5] Xiao X, Long A, Zeng X (2014) Through-thickness permeability modelling of woven fabric under out-of-plane deformation. J Mater Sci 49:7563–7574. https://doi.org/10.1007/s10853-014-8465-z

[6] Pazmino J, Mathieu S, Carvelli V, Boisse P, Lomov SV (2015) Numerical modelling of forming of a non-crimp 3D orthogonal weave E-glass composite reinforcement. Compos A 72:207–218

[7] Potluri P, Manan A (2007) Mechanics of non-orthogonally interlaced textile composites. Compos A 38(4):1216–1226

[8] Daelemans L, Faes J, Allaoui S, Hivet G, Dierick M, Van Hoorebeke L, Van Paepegem W (2016) Finite element simulation of the woven geometry and mechanical behaviour of a 3D woven dry fabric under tensile and shear loading using the digital element method. Compos Sci Technol 137:177–187

[9] Kyosev Y (2018) Numerical modelling of 3D braiding machine with variable paths of the carriers. Appl Compos Mater 25(4):773–783

[10] Ghazimoradi M, Alamda-Yazdi AA, Yazdanshenas ME (2014) Evaluation of the fabric formability by concentrated loading method. J Text Polym 2:56–59

[11] Quek SC, Waas AM, Shahwan KW, Agaram V (2003) Analysis of 2D triaxial flat braided textile composites. Int J Mech Sci 45(6–7):1077–1096

Accepted Manuscript

[12] Mamiliano D (2002) Tetraxial fabric and machine for its manufacture. European patent EP1412570. Tetraxial S.r.l., Milano, IT

[13] Lomov SV, Ivanov DS, Verpoest I, Zako M, Kurashiki T, Nakai H, Hirosawa S (2007) Meso-FE modelling of textile composites: road map, data flow and algorithms. Compos Sci Technol 67(9):1870–1891

[14] Potluri P, Parlak I, Ramgulam R, Sagar TV (2006) Analysis of tow deformations in textile preforms subjected to forming forces. Compos Sci Technol 66(2):297–305

[15] Badel P, Vidal-Sallé E, Boisse P (2007) Computational determination of in-plane shear mechanical behaviour of textile composite reinforcements. Comput Mater Sci 40(4):439–448

[16] Naouar N, Vidal-Sallé E, Schneider J, Maire E, Boisse P (2014) Meso-scale FE analyses of textile composite reinforcement deformation based on X-ray computed tomography. Compos Struct 116:165–176

[17] El Said B, Ivanov D, Long AC, Hallett SR (2016) Multi-scale modelling of strongly heterogeneous 3D composite structures using spatial Voronoi tessellation. J Mech Phys Solids 88:50–71

[18] Badel P, Vidal-Sallé E, Boisse P (2008) Large deformation analysis of fibrous materials using rate constitutive equations. Comput Struct 86(11–12):1164–1175

[19] Charmetant A, Vidal-Sallé E, Boisse P (2011) Hyperelastic modelling for mesoscopic analyses of composite reinforcements. Compos Sci Technol 71(14):1623–1631

[20] Gong Y, Peng X, Yao Y, Guo Z (2016) An anisotropic hyperelastic constitutive model for thermoplastic woven composite prepregs. Compos Sci Technol 128:17–24

[21] Yao Y, Huang X, Peng X, Liu P, Youkun G (2017) An anisotropic hyperelastic constitutive model for plain weave fabric considering biaxial tension coupling. Text Res J. https://doi.org/10.1177/0040517517748495

[22] Ciarlet PG (1988) Mathematical elasticity volume I: three-dimensional elasticity. North Holland, Amsterdam

[23] Marsden JE, Hughes TJR (1993) Mathematical foundations of elasticity. Dover Publications Inc, New York

[24] Boehler JP (1978) Lois de comportement anisotrope des milieux continus. J de Mèc 17:153–190

[25] Itskov M (2000) On the theory of fourth-order tensors and their applications in computational mechanics. Comput Methods Appl Mech Eng 189:419–438

[26] Quanshui Z, Boehler J (1994) Tensor function representations as applied to formulating constitutive laws for clinotropic materials. Acta Mech Sin 10:336–348

[27] Obert E, Daghia F, Ladevèze P, Ballere L (2014) Micro and meso modeling of woven composites: Transverse cracking kinetics and homogenization. Compos Struct 117(1):212–221

[28] Carvelli V, Poggi C (2001) A homogenization procedure for the numerical analysis of woven fabric composites. Compos A 32(10):1425–1432

[29] Abaqus 6.14 (2014) User manual, Dassault Systèmes Simulia Corp., Provid. RI, USA

[30] Ghazimoradi M, Carvelli V, Marchesi MC, Frassine R (2018) Mechanical characterization of tetraxial textiles. J Ind Text 48(1):3–24

[31] Correlated Solutions, Inc. (2012) VIC-2D, Irmo, SC, USA, www.correlatedsolutions.com. Accessed Nov 2017

Accepted Manuscript